Targeted Upregulation of *PKD1/PKD2* with Programmable PPR Proteins: A Versatile Approach for Addressing Haploinsufficiency

By: Carl Andersen Tan 1AG21231S

Laboratory: Genome Chemistry Engineering Supervisor: Prof. Nakamura Takahiro Faculty of Agriculture (IUPE)



Abstract

Autosomal Polycystic Kidney Disease (ADPKD) remains one of the most common genetic disorders worldwide, arising from haploinsufficiency of *PKD1/2* genes. This study engineered synthetic RNA-binding pentatricopeptide repeat (PPR) proteins fused to the translational scaffold eIF4G to induce *PKD1/PKD2* expression through two synergistic mechanisms: (1) blockade of inhibitory elements, and (2) direct recruitment of translational machinery. When the translational enhancement of PPR-eIF4G constructs was evaluated in mammalian cultured cells, we obtained a 4-fold increase in *PKD1* mRNA (p<0.001), 1.6-fold upregulation of PC1 (p<0.01), and a 3-fold increase of PC2 (p<0.0001), demonstrating potential for translational enhancement therapy. The efficacy of targeted upregulation proved to be highly site dependent. Most intervention sites including putative microRNA regulatory elements failed to enhance translation despite inducing robust mRNA upregulation. This precise target sequence or positional requirement establishes target site optimization as a key therapeutic challenge for PPR-eIF4G mediated translational enhancement.

Table of Contents

I.	Introduction	4
a.	. Overview of Autosomal Dominant Polycystic Kidney Disease	4
b. <i>F</i>	. Regulation of PKD1 and PKD2 by MicroRNAs (miRNA) and Upstream Open Reading rames (uORF)	4
c.	. Translational Enhancement Using Pentatricopeptide Proteins (PPR)	5
II.	Results	7
a.	. Design and validation of PPR-eIF4G proteins targeting PKD1 and PKD2	7
b.	. PKD1 5' and 3' UTR targeting PPR-eIF4G drives translational enhancement10	0
C.	. PKD2 5'UTR targeting PPR-eIF4G drives robust translational enhancement12	2
d	. PPR-eIF4G expression enhances PKD1 mRNA levels through microRNA blocking13	3
III.	Discussion15	5
a.	. Therapeutic significance of PKD1/PKD2 upregulation1	5
b.	. PPR-elF4G target sensitivity16	6
C.	Discrepancy between mRNA and protein expression in PC1 from miR-200 blocking onstructs16	6
IV.	Conclusion18	8
V.	Materials and Methods19	9
a.	. Construction of programmable PPR protein gene19	9
b.	. Construction of PPR-eIF4G fusion expression vector19	9
c.	. Cell culture and cell transfection19	9
d	. RNA extraction and cDNA synthesis20	0
e.	. Real-time quantitative polymerase chain reaction (RT-qPCR)20	0
f.	Western blot analysis20	0
g.	Enzyme linked immunoassay (ELISA) for polycystin-1 and polycystin-22	1
h.	. Statistical analysis2	1
VI.	Bibliography22	2
VII.	Supplementary information20	6

I. Introduction

a. Overview of Autosomal Dominant Polycystic Kidney Disease

Autosomal Dominant Polycystic Kidney Disease (ADPKD) is among the most prevalent monogenic disorders globally, affecting an estimated 12 million individuals and representing the fourth leading cause of end-stage renal disease. The disease is characterized by the development of multiple cysts in the kidneys, associated with a gradual decline in renal function¹. The primary genetic drivers of ADPKD are loss-of-function mutations in *PKD1* (encoding Polycystin-1; PC1) and *PKD2* (encoding Polycystin-2; PC2) genes which account for ~85% and ~15% of cases, respectively ². PC1 and PC2 forms a calcium permeable transmembrane protein complex localized within primary cilia of renal epithelial cells ³. This complex is critical for cilia-mediated Ca²⁺ signaling, cell cycle regulation, and tubular morphogenesis, with dysfunction leading to aberrant cell proliferation, and ultimately cyst formation ³.

Although loss of function mutations in *PKD1* and *PKD2* drive ADPKD progression, disease development involves mechanisms beyond monogenic inheritance. The 'two-hit' model posits that ADPKD develops due to a germline mutation in one allele of the PKD gene, followed by a somatic mutation in the remaining wild-type allele, leading to the complete loss of functional polycystin⁴. While the two-hit model explains focal cystogenesis, somatic second hits are not universally detected suggesting other alternative mechanisms⁵. To explain ADPKD development in absence of the somatic second hit, the gene dosage model suggests that cystogenesis arises when levels of functional PC1 or PC2 fall below a critical threshold due to haploinsufficiency⁶. Hence, a germline mutation alone may suffice to reduce polycystin levels beyond the critical threshold required for renal maintenance, thereby resulting in cyst formation. This haploinsufficiency underscores the sensitivity of polycystin levels encoded by genes *PKD1* and *PKD2* for physiological tubular maintenance.

b. Regulation of PKD1 and PKD2 by MicroRNAs (miRNA) and Upstream Open Reading Frames (uORF)

Like many genes, *PKD1* and *PKD2* are tightly regulated through an interplay of transcriptional, translational, and post-translational mechanisms. miRNAs, and uORFs play key roles in controlling the stability and translation efficiency of the PKD genes. MicroRNAs are a class of small RNA sequences (~22 nucleotides) that bind to complementary sequences usually within the 3' untranslated region (UTR) of the target mRNA. miRNA inhibit expression of target genes primarily through translational repression, or mRNA degradation⁷. miR-17 and miR-200 bind to complementary sequences within 3' UTR regions of *PKD1* and *PKD2*, inhibiting their expression and leading to cystogenesis ⁸⁻¹⁰. This repression is further exacerbated as miR-17 is upregulated in human and murine models with ADPKD¹¹.

Upstream open reading frames (uORF) are short ORFs that reside within the 5'UTR. uORFs regulate (usually repress) gene expression at the transcriptional or post transcriptional level through a variety of mechanisms. uORF can prevent translational initiation at the main ORF leading to

ribosomal-stalling, leaky scanning, production of nonfunctional peptides, or mRNA degradation through nonsense mediated decay¹². The 5' UTR of PKD genes contains uORFs that repress expression of functional polycystin^{13,14}.

Given their inhibitory role, miRNA and uORF act as negative regulators of polycystin expression and are key targets for ADPKD therapy. Blocking and knockout experiments of miRNA binding sites as well as uORFs in PKD genes have demonstrated that disruption of these regulatory elements can reverse this repression. In multiple orthologous mouse ADPKD models, knockout of miR-17 binding site in *PKD1* and 2 improved expressions of PC1 and PC2, decreased kidney injury biomarkers, and ultimately attenuated cyst growth. Furthermore, treatment of mouse models with anti-miR-17 ASO halted ADPKD development and stabilized tubular function⁸. In another study, deletion of the uORF in both PKD genes resulted in respective increase of expression of PC1 and PC2¹³. However, when the study investigated blocking of the *PKD1* uORF using ASOs, they found reduced PC1 level. It was noted that 'blocking' of the *PKD1* uORF with ASOs potentially led to stabilizations of 5'UTR RNA structures that made the uORF more effective at repressing translation akin to Class I uORF-ASOs^{12,13}.

c. Translational Enhancement Using Pentatricopeptide Proteins (PPR)

Gene manipulation technology offers a powerful avenue for creating therapeutic solutions to ADPKD. Previous studies have employed knockout strategies and ASO-mediated blocking to repress inhibitory elements in PKD1/PKD2, thereby reversing haploinsuffiency of PC1 and PC2. However, each approach carries distinct limitations. DNA editing techniques such as CRISPR/Cas nucleases has been widely employed in knockout strategies to insert or remove targeted DNA sequences. While powerful, the usage of CRISPR/Cas nucleases reportedly caused unexpected genomic mutations, mosaicism, and off target effects, resulting in potentially dangerous and irreversible changes to the genome 15. For this reason, RNA-based manipulation technologies provide an attractive avenue for development of safe genetic therapies. They provide reversible, and precise control of genetic information, making it a favorable therapeutic option for ADPKD. A leading example is RGLS4326, an anti-miR-17 ASO developed for ADPKD. RGLS4326 enhances polycystin expression, attenuated cystogenesis in murine models, and minimal off-target effects with favorable safety margins 16. Despite these advances, ASOs have several limitations when applied for translational enhancement. ASOs can unpredictably alter mRNA structures, resulting the formation of secondary structures that stabilize inhibitory sequences as with class I uORF-ASOs¹⁷. In addition, ASOs and other RNA interference (miRNA/siRNA) are limited to blocking repressive effects of inhibitory sequences, rather than the direct induction of translation¹⁸.

Pentatricopeptide Proteins (PPR) are sequence specific RNA binding proteins involved in the stability, processing, splicing, and editing of various RNA¹⁹. In contrast to ASOs or other gRNA nucleotide-based systems, PPR proteins recognize specific RNA sequences through variable repeating PPR motifs. PPR form long scaffolds comprising smaller PPR motifs, each recognizing a nucleotide of the target mRNA. The nucleotide specificity of each PPR motif is determined by the amino acid on the 2nd, 5th, and 35th positions, while the PPR target length is dictated by the number of motifs^{20,21}. This modular architecture enables PPR proteins to bind their target sequences with

higher specificity, with longer PPR scaffold chains more tolerant to mismatches, distinguishing between bases more effectively than canonical Watson-Crick base pairing²²⁻²⁴. In addition to high programmability, PPR proteins have been previously fused with protein effectors to induce site specific nucleotide base substitutions, splicing, cleavage, and translational enhancement^{21,25,26}. A previous study demonstrated that PPR proteins fused to the translational initiation scaffold protein eIF4G can enhance translation of endogenous mRNAs in cultured animal cells²⁶. In the current study, 12motif PPR proteins are employed to suppress inhibitory sites within the 5' and 3' UTR, while utilizing PPR-eIF4G fusions to specifically enhance expression of *PKD1/PKD2*. This PPR-based technology represents a promising novel therapeutic approach for correcting haploinsufficiency in genetic disorders such as autosomal dominant polycystic kidney disease.

II. Results

a. Design and validation of PPR-eIF4G proteins targeting PKD1 and PKD2

To enhance endogenous expression of *PKD1* and *PKD2*, we incorporated a dual targeting strategy using PPR proteins: (1) simultaneous competitive inhibition of repressive elements within *PKD1/PKD2* 5' and 3' UTRs and (2) Translational activation via PPR-eIF4G fusions that recruit translational initiation factors to target RNA^{26,27} (Fig.1). Our design incorporates a truncated eIF4G scaffold (607–1600 aa), previously shown to enhance endogenous mRNA expression, while coupling uORF and miRNA site inhibition to synergistically boost polycystin expression.

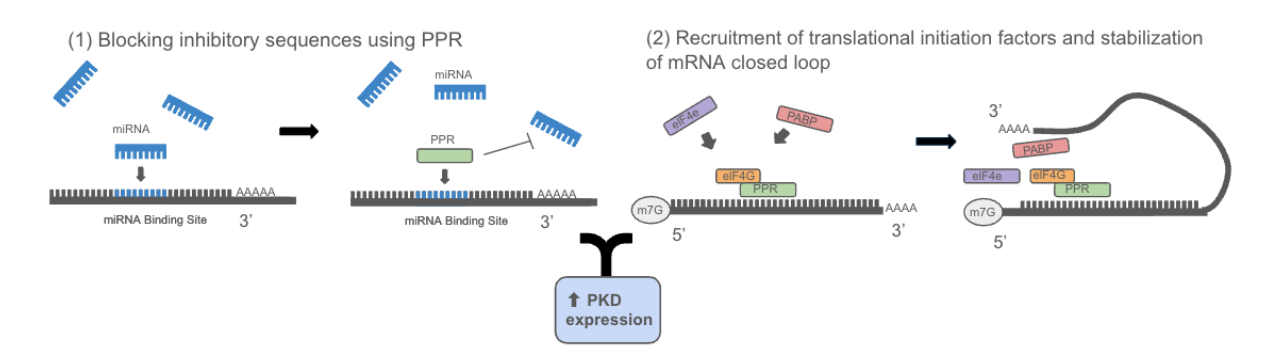


Figure 1. Conceptual framework of translational enhancement using simultaneous PPR blocking of inhibitory elements, and recruitment of translation initiation factors via eIF4G.

We selected 22 and 16 distinct 12-nucleotide target sequences within PKD1 and PKD2 mRNA respectively (Table 1,2). Most PPR targets were spaced evenly along target 5' and 3' UTR, while others targeted specific inhibitory sequences including miRNA binding site and upstream open reading frame (uORF). Predicted miRNA binding sites were identified through miRBase (v22)²⁸ and TargetScanHuman 8.0²⁹ focusing on conserved miRNA family binding clusters, while regulatory uORFs in PKD2 were identified from published studies¹⁴. The designer PPR gene was cloned with Nterminal 3xFlag tag and a C-terminal eIF4G into a CMV promoter-controlled expression vector (Fig. 2A). To ensure PPR-eIF4G expression vectors were constructed correctly, all constructs were validated by insert size confirmation (Fig. S1A), restriction enzyme digestion analysis (Fig. S1B), and Sanger sequencing. The designer PPR protein was transiently transfected into HEK293T cells, and western blot analysis of cell lysates confirmed successful robust expression of 3xFlag-tagged PPReIF4G fusion proteins at their predicted molecular weights with no expression in mock or nontransfected cells (Fig. 2B). To establish optimal cell harvest time, we conducted a time-dependency analysis of PPR expression. Cells transfected with 3xFlag-tag constructs were harvested at 24, 48, 72, and 96hrs post transfection. Western Blot analysis revealed peak accumulation at 48hrs with declining expression at 72 and 96hrs (Fig. 2C). Based on these results, subsequent experiments used a standardized 48-hour post-transfection harvest protocol.

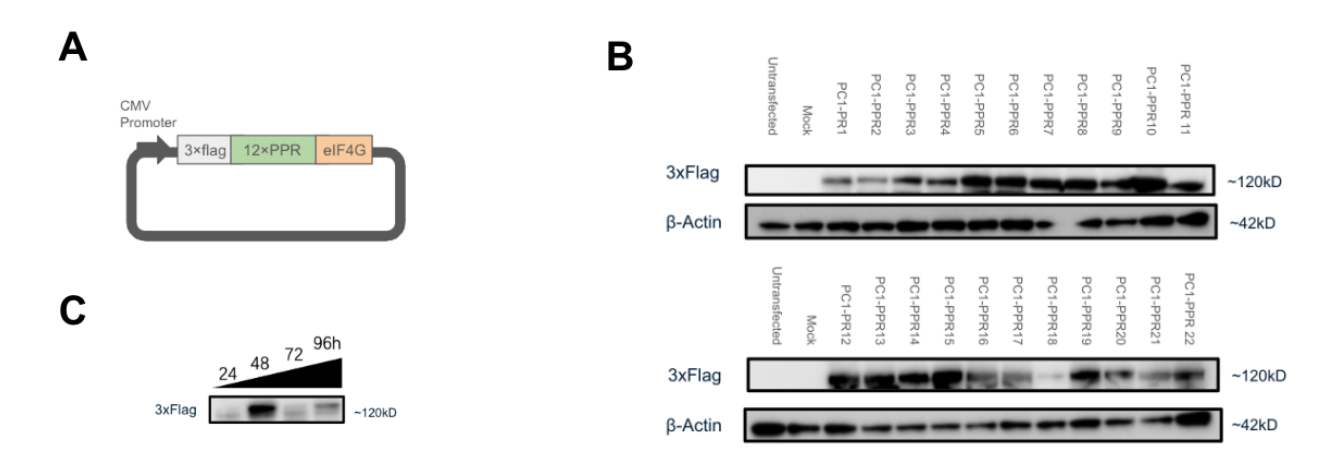


Figure 2. Design and construction of pentatricopeptide repeat (PPR)-eIF4G fusion protein. (A) Structure of PPR-eIF4G expression vector. The PPR protein gene with 12 PPR motifs (for 12nt recognition) was fused with 3×FLAG and truncated eIF4G and integrated in plasmid under the CMV promoter. (B) Western blot analysis using anti-FLAG antibody to examine expression of PPR-eIF4G plasmid in the absence (mock and untransfected controls)

or in the presence of PC1 targeting expression vectors (PC1-PPR). β-actin was used as an internal control. Mock refers to empty vector transfected controls. (C) Western blot using anti-FLAG antibody to examine expression levels of the

PPR protein in HEK293T cells 24, 48, 72, or 96hrs post-transfection.

Table 1: Target region, position, and sequence of *PKD1* targeting eIF4G PPR constructs.

PPR Construct	Region (PKD1)	PKD1 mRNA Position	Targeting Sequence
PC1-PPR1	5' UTR (start)	203-214	GCCCUAACGAUG
PC1-PPR2	5' UTR	175-186	CUGGGGACGGCG
PC1-PPR3	5' UTR	146-157	UGAGCUGCGGUC
PC1-PPR4	5' UTR	117-128	CGCCCGCCAUGC
PC1-PPR5	5' UTR	89-100	CGCGGCCGCGCA
PC1-PPR6	5' UTR	61-72	CCCGAGCGGGCG
PC1-PPR7	5' UTR	33-44	GAGCUCCCGGAG
PC1-PPR8	5' UTR (end)	1-12	GCACUGCAGCGC
PC1-PPR9	3' UTR (start)	13,112-13,113	CCUCCUUCCUGG
PC1-PPR10	3'UTR	13,265-13,276	GGCUUCAGCACU
PC1-PPR11	3' UTR	13,408-13,419	GCUGUGCCCGGC
PC1-PPR12	3' UTR	13,551-13,562	GUGUGUCUCGUG
PC1-PPR13	3' UTR	13,694-13,705	CAGCCCGGCUGC
PC1-PPR14	3' UTR	13,837-13,848	GCUGGCAUCAGG
PC1-PPR15	3' UTR	13,980-13,991	GAGUGUGCUGUA
PC1-PPR16	3' UTR (end)	14,125-14,136	CUGUCUGACUGC
PC1-PPR17	miR-17 blocking (1)	13,268-13,279	UUCAGCACUUUA
PC1-PPR18	miR-17 blocking (2)	13,270-13,281	CAGCACUUUAAA
PC1-PPR19	miR-17 blocking (3)	13,272-13,283	GCACUUUAAAGA
PC1-PPR20	miR-200 blocking (1)	13,336-13,347	GACACAGCAGUA
PC1-PPR21	miR-200 blocking (2)	13,339-13,350	ACAGCAGUAUUG
PC1-PPR22	miR-200 blocking (3)	13,342-13,353	GCAGUAUUGGAC

Table 2: Target region, position, and sequence of *PKD2* targeting eIF4G PPR constructs.

PPR Construct	Region (PKD2)	PKD2 mRNA Position	Targeting Sequence
PC2-PPR1	5'UTR (start)	1-12	AGGCGGCGG
PC2-PPR2	uORF blocking (1)	31-41	ACAUGGCUCCUG
PC2-PPR3	5'UTR	59-70	CGCGGCGCCGCG
PC2-PPR4	5'UTR (end)	91-102	GUGACCGCGAUG
PC2-PPR5	uORF blocking (2)	24-35	AAAGGAACAUGG
PC2-PPR6	uORF blocking (3)	27-38	GGAACAUGGCUC
PC2-PPR7	3'UTR (start)	3,009-3,020	UGUGUGUUUCAG
PC2-PPR8	3'UTR	3,699-3,710	UCAGUUAUAGGA
PC2-PPR9	3'UTR	3,874-3,885	GUGACAUUUUGA
PC2-PPR10	3'UTR (end)	4,035-4,046	GAUAUAGUAGCA
PC2-PPR11	miR-17 (1) blocking	4,389-4,400	CUGCACUUUAAU
PC2-PPR12	3'UTR	5,078-5,089	UCUAGUGAGACC
PC2-PPR13	3'UTR	3,136-3,147	CGCCUGUAAUCC
PC2-PPR14	miR-140 blocking	4,767-4,778	UAUGUGGUAUCC
PC2-PPR15	miR-183 blocking	4,792-4,803	AUGUGCCAUAUA
PC2-PPR16	miR-17 (2) blocking	5,051-5,062	GAGCACUUUACU

b. PKD1 5' and 3' UTR targeting PPR-eIF4G drives translational enhancement

We engineered 22 distinct PPR-eIF4G constructs designed to target various regions of *PKD1* mRNA (Fig. 3A). To assess whether transfection of PPR-eIF4G constructs enhanced expression of PC1, we performed both western blot and ELISA analysis. Initial western blotting of cell lysates failed to detect full length PC1 (460kDa) due to technical challenges associated with large membrane protein extraction, protein transfer, or possible degradation of protein as evidenced by an unexpected immunoreactive ~80kDa band (potentially a PC1 cleavage product or PC1 precursor variant) (Fig. S2A). Given this limitation, we employed ELISA for PC1 detection and quantification.

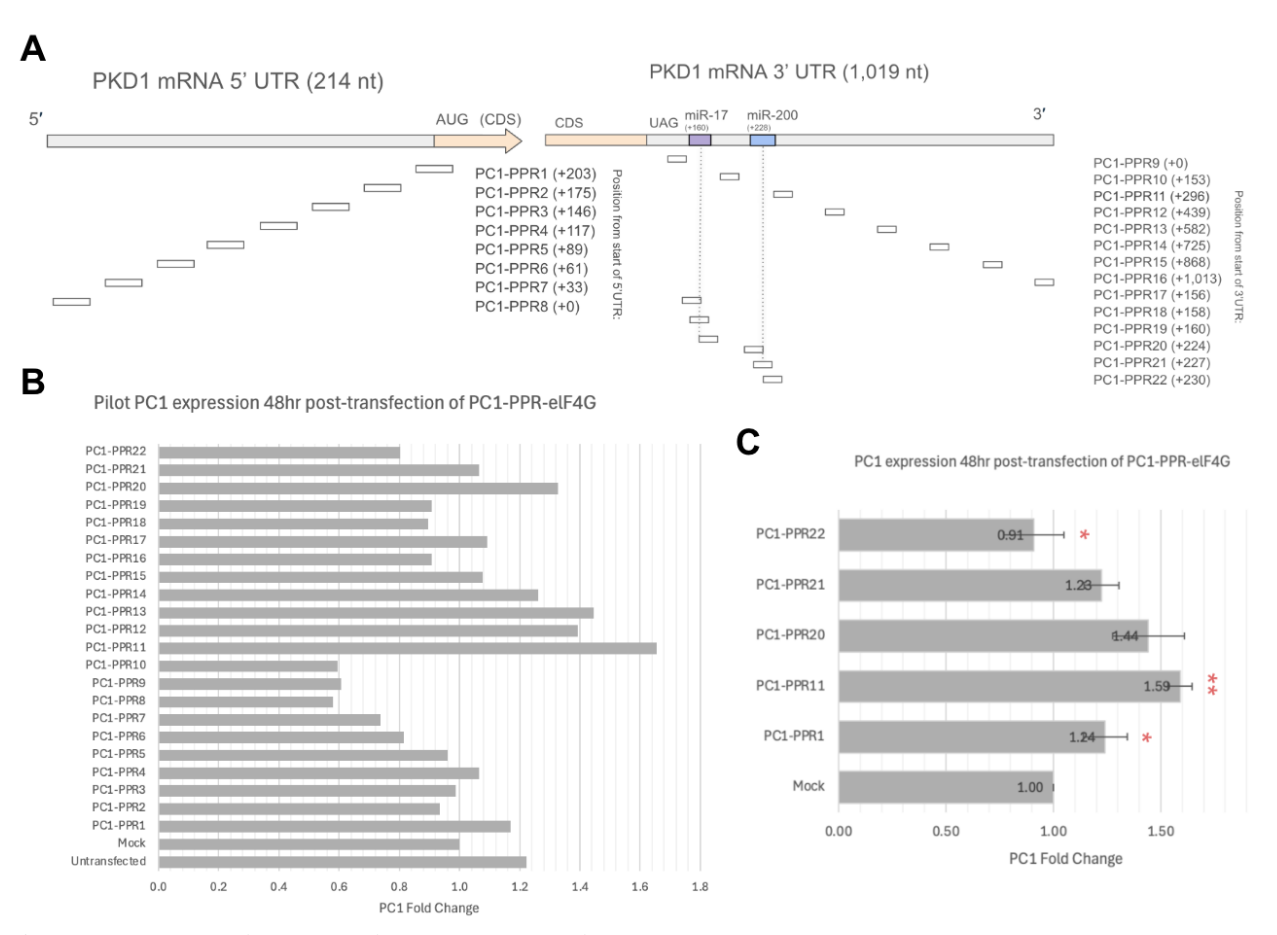


Figure 3. *PKD1* Protein (Polycystin-1, PC1) Translational Enhancement **(A)** *PKD1* 5' and 3' UTR and target position of designed PPR-eIF4G fusion gene (PC1-PPR1 to PC1-PPR22). **(B)** Screening for PC1 protein accumulation in *PKD1* targeting PPR-eIF4G. PC1 protein level was analyzed in HEK293T cells by ELISA assay 48hrs after transfection (N=1). **(C)** Translational enhancement of PC1 in selected PPR-eIF4G targets. Unpaired two-tailed Student's t-test (N=3, *p<0.05, **p<0.01). Error bar indicates the standard deviation between biological replicates.

A preliminary screening (n=1) was conducted to optimize lysate loading concentrations, and to select promising PPR-eIF4G candidates for further analyses. The quantitative ELISA assay established 20 ng of total lysate protein was sufficient for PC1 detection for the assay's range. Candidate selection was based on the magnitude of PC1 upregulation compared to mock (Fig. 3B),

and position of target sites. PC1-PPR1 was chosen as 5'UTR-targeting candidate, PC1-PPR11 as 3'UTR-targeting, and PC1-PPR20/21/22 as functional element inhibitory constructs for further evaluation.

With the next evaluation using ELISA, candidates revealed position-dependent effects of PPR-eIF4G constructs on PC1 concentration. Transfection with PC1-PPR11 (3'UTR targeting) and PC1-PPR1 (5'UTR targeting) resulted in 1.6-fold increase (p<0.01) and 1.2-fold increase (p<0.05) in PC1 respectively (Fig. 3C). Notably, both constructs enhanced translation despite binding to arbitrary UTR sites devoid of known regulatory elements. This suggests eIF4G mediated translational enhancement, independent of repressive element blockade. All ELISA reactions demonstrated excellent linearity (R>0.99; Fig. S2B).

c. PKD2 5'UTR targeting PPR-eIF4G drives robust translational enhancement

The same experimental approach for evaluation of PC1 translational enhancement was used to evaluate PC2. A total of 16 distinct PPR-eIF4G constructs were designed to target various regions of *PKD1* mRNA (Fig. 4A). Quantitative ELISA revealed a potent position-dependent PC2 upregulation mediated by 5'UTR targeting constructs (Fig. 4B). Analysis of 5'UTR constructs revealed complex positional effects on PC2 expression that could not be explained by proximity from the 5' cap. The most robust increases were observed in PC2-PPR1 (3.1-fold, p<0.01), PC2-PPR2 (3.0-fold, p<0.0001), and PC2-PPR3 (2.7-fold, p<0.001). Additional western blot analysis of full length PC2 (~110kDa) confirmed these findings, showing band intensities that correlated well with the results from quantitative ELISA (Fig. 4C).

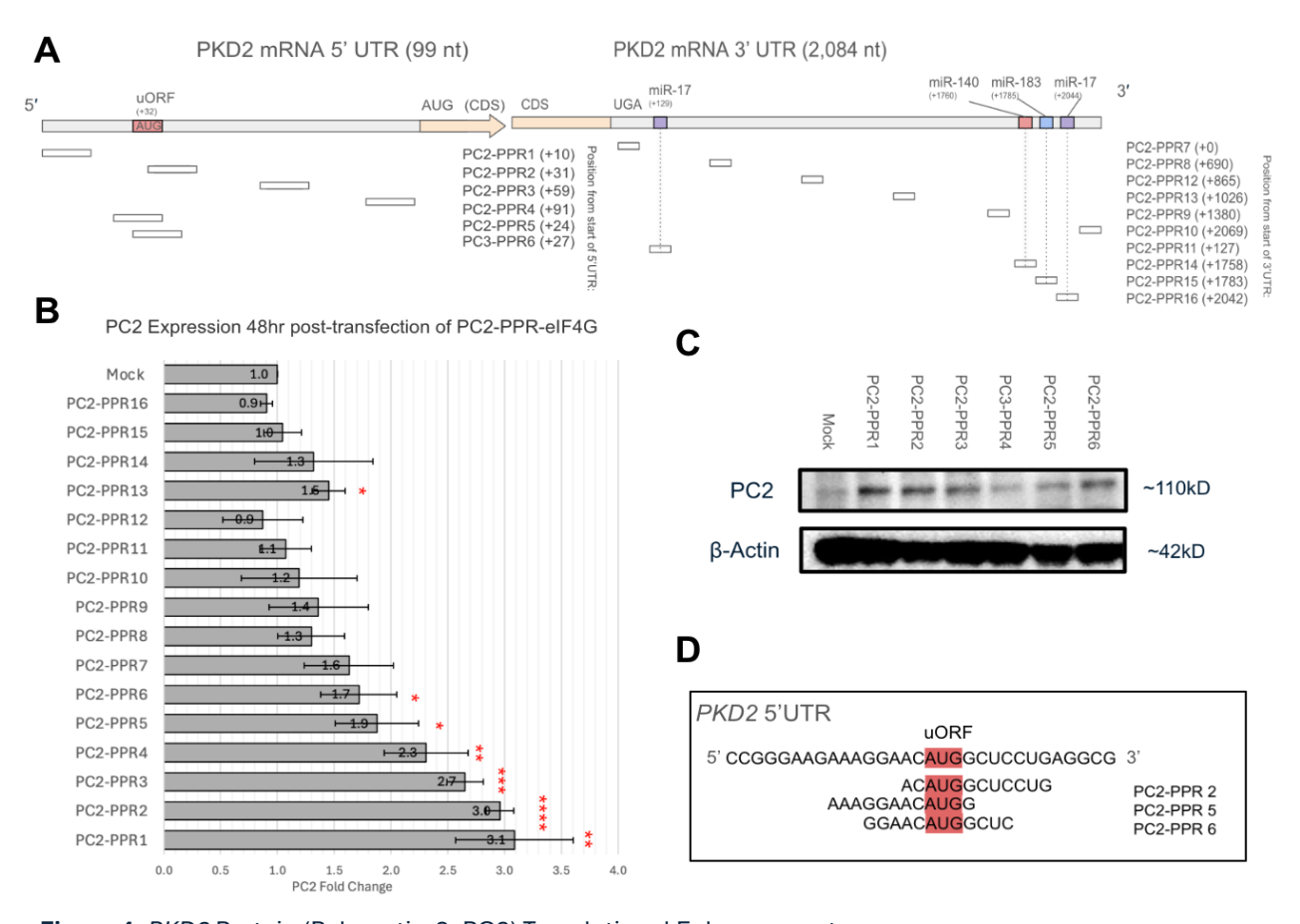


Figure 4. PKD2 Protein (Polycystin-2, PC2) Translational Enhancement (A) PKD1 5' and 3' UTR and target position of designed PPR-eIF4G fusion gene (PC2-PPR1 to PC2-PPR16). (B) PC2 protein accumulation in PKD2 targeting PPR-eIF4G. PC2 protein level was analyzed in HEK293T cells by ELISA assay 48hrs after transfection. Unpaired two-tailed Student's t-test (N=3, *p<0.05, **p<0.01). Error bar indicates the standard deviation between biological replicates. (C) Western blot analysis using anti-polycystin-2 antibody). β-actin was used as an internal control. (D) Target position and overlap of uORF blocking PPR in PKD2 5'UTR.

Interestingly, PC2-PPR2, PC2-PPR5 and PC2-PPR6 were all designed to block an uORF in the 5'UTR yet showed markedly different magnitudes of enhancement (3.0-fold, 1.9-fold and 1.7-fold respectively, all p<0.05; Fig. 4D). This differential effect suggests that while uORF blockade may contribute to PC2 upregulation, it is unclear whether results could also be attributed to the positional dependency of PPR-eIF4G mediated translational enhancement. Constructs targeting the 3'UTR produced minimal (PC2-PPR13; 1.5-fold, p<0.05) or no significant increase in PC2 concentration, underscoring the importance of target selection, particularly 5'UTR engagement in *PKD2* translational enhancement. All ELISA reactions demonstrated excellent linearity (R>0.99; Fig. S3).

d. PPR-eIF4G expression enhances PKD1 mRNA levels through microRNA blocking

To determine whether PPR-eIF4G could counteract canonical miRNA gene silencing mechanisms —which typically induces mRNA transcript degradation—we analyzed *PKD1* and *PKD2* mRNA levels following transfection with 6 *PKD1*-targeting and 4 *PKD2*-targeting miRNA-blocking PPR constructs. RT-qPCR revealed PPR-eIF4G-mediated stabilization of *PKD1* transcripts through miRNA interference. miR-200 blocking constructs functionally inhibited miR-200 activity, leading to robust upregulation of *PKD1* mRNA. PC1-PPR22 induced an approximately four-fold increase in *PKD1* mRNA compared to mock-transfected controls at 48hrs after transfection (p<0.001;Fig. 5A). Similarly, PC1-PPR21 which also targeted the miR-200 binding site markedly showed a three-fold induction (p<0.01).

Notably, while PC1-PPR21 and PC1-PPR22 successfully upregulated *PKD1* mRNA expression, other constructs targeting overlapping miR-200 exhibited divergent effects. PC1-PPR20 which binds only three nucleotides downstream of PC1-PPR21 target sequence failed to elevate *PKD1* mRNA levels (p>0.01). This stark contrast highlights the positional sensitivity of PPR-RNA interactions, where even minor shifts (~3nt) in target binding sites can critically impact PPR blocking. Similarly, PPR constructs (PC1-PPR17 to PC1-PPR19) targeting miR-17 binding sites showed no change in *PKD1* transcript levels, underscoring the requirement that PPR-eIF4G mediated RNA upregulation requires optimal target site selection for the blockade of regulatory elements, rather that non-specific transcriptional activation.

This observed target-site specificity extends to PKD2, where PPR-eIF4G constructs targeting predicted miRNA binding sites showed no significant upregulation of PKD2 RNA (p>0.05; Fig. 5B). This can suggest a similar ineffective targeting of putative miRNA binding sites, or miRNA-mediated regulation may primarily operate post transcriptionally through translational silencing rather than RNA degradation consistent with established inhibitory mechanisms of miR-17^{10,11}. All RT-qPCR primers exhibited satisfactory amplification efficiency (R > 0.99; Fig. S4) with all Ct values normalized to β -actin as housekeeping gene.

Beyond target specificity, we made a striking observation regarding miR-200 targeting constructs. Despite achieving a 3-4-fold increase in *PKD1* mRNA, PC1-PPR21/PPR22 failed to enhance PC1 expression (p>0.05), revealing a critical disconnect between transcript abundance and protein output. Systematic analysis of other miRNA blocking constructs revealed no correlation between mRNA and protein levels (R²=0.04; Fig. 5C), strongly suggesting the presence of other regulatory mechanisms of miRNA blockade on PC1 translation.

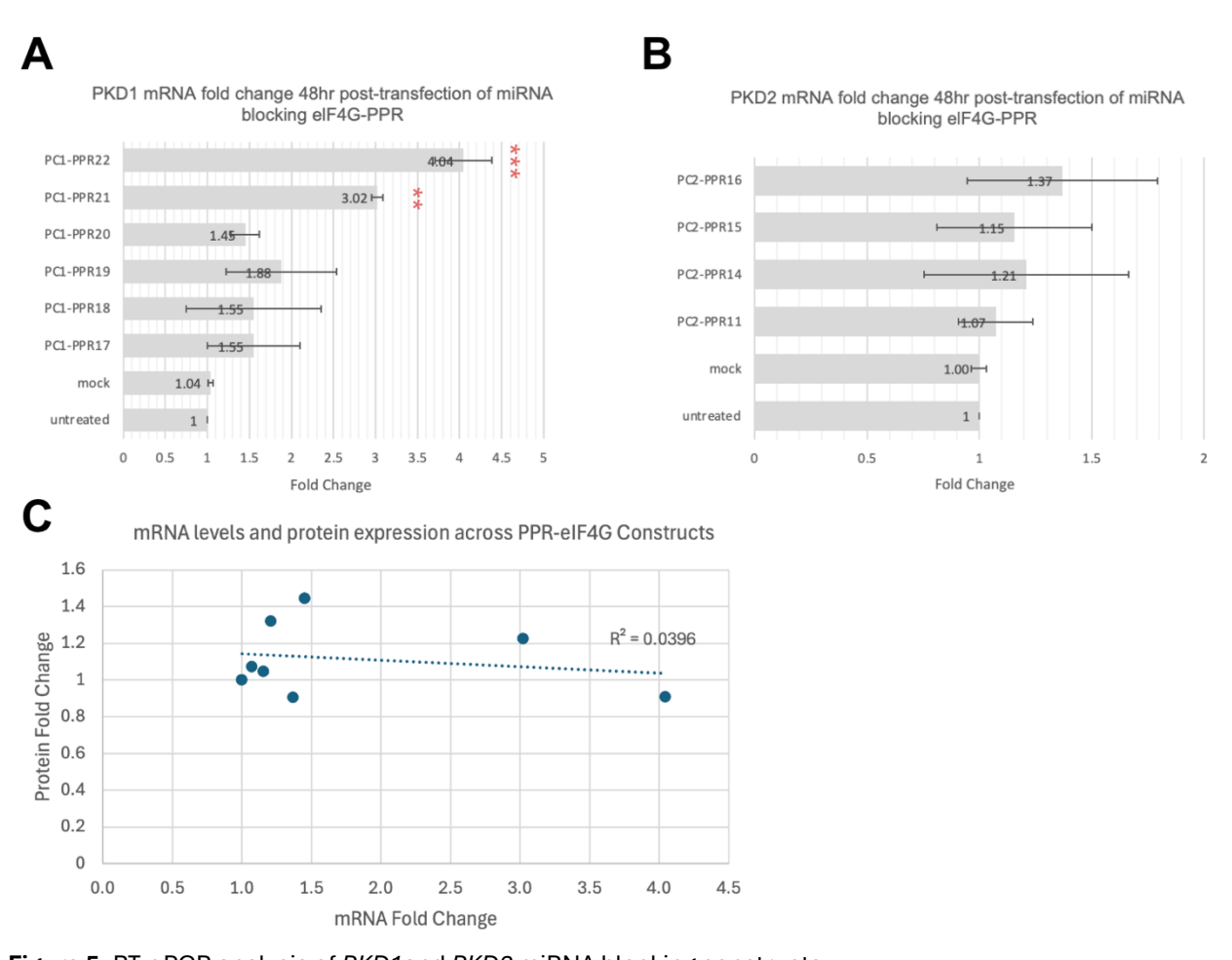


Figure 5. RT-qPCR analysis of *PKD1* and *PKD2* miRNA blocking constructs (A) *PKD1* mRNA expression in *PKD1* miRNA blocking constructs (PC1-PPR17 to PC1-PPR22) compared to mock. β-actin was used as housekeeping gene. Unpaired two-tailed Student's t-test (N=3, **p<0.01, ***p<0.001). Error bar indicates the standard deviation between biological replicates. (B) *PKD2* mRNA expression in *PKD2* miRNA blocking constructs (PC2-PPR11, PC2-PPR14 to PC1-PPR16) compared to mock. Analysis conducted same as (A). (C) Scatter plot of mRNA and protein abundance across miRNA blocking constructs

III. Discussion

a. Therapeutic significance of PKD1/PKD2 upregulation

This study demonstrates that PPR-eIF4G fusion proteins effectively enhance *PKD1* and *PKD2* protein expression to therapeutically relevant levels, achieving 1.6-fold (PC1) and 3.0-fold (PC2) increases. These expression levels match or exceed those previously shown to restore renal function and inhibit ADPKD progression in mouse models. These results establish PPR-eIF4G as a viable strategy for reaching the polycystin expression thresholds required for therapeutic benefit in ADPKD.

The haploinsufficiency model of ADPKD suggests that a theoretical 2-fold increase in *PKD1/PKD2* should restore expression to wild-type levels, thus compensating for the disease-causing allele. However, emerging evidence demonstrates that even sub-physiological increases in PC1 can significantly modify ADPKD progression^{30,31}. Murine models highlight the nonlinear relationship between polycystin-1 dosage and phenotypic severity. ADPKD murine models with 40% PC1 expression develop rapid cystogenesis, profound decline in renal function, and reduced survival, reflecting aggressive human ADPKD^{32,33}. Conversely, maintaining PC1 at 60-80% of normal expression permits long-term viability with gradual cyst development, demonstrating that small differences in PC1 dosage above the haploinsufficiency threshold (50%) can confer protection. This aligns with clinical observations where residual PC1 function and dosage correlates with delayed end stage renal disease (ESRD) onset³⁴. Small differences in PC1 dosage have outsized effects, suggesting that our observed 1.6-fold upregulation, though seemingly modest, can significantly modify ADPKD disease trajectory.

This dosage sensitivity extends to *PKD2*, where murine knockout models demonstrated that even a 2-fold increase in PC2 expression via transgenic rescue can significantly mitigate ADPKD phenotypes, resulting in reduced cyst formation, improving renal function, and doubling median survival³¹. Importantly, the study found that a 3-fold increase in PC2 nearly suppresses ADPKD development achieving minimal or no cyst formation, normalized kidney biomarkers, and restored survival. Furthermore, this degree of overexpression did not result in abnormal development or decreased survival in healthy mice, hence alleviating concerns about potential toxicity of supraphysiological levels of PC2. Our PPR-mediated approach thus achieves a therapeutic "sweet spot" providing enhancement sufficient to overcome haploinsufficiency, while avoiding potential overexpression toxicity.

This study demonstrates that PPR-eIF4G fusions achieve clinically meaningful polycystin upregulation (1.6-fold PC1, 3.0-fold PC2) within established therapeutic windows. Unlike transgenic approaches, PPR-based enhancement eliminates risks of genomic disruption or long-term PC1 or PC2 overexpression toxicity observed in viral transgene systems³⁵. The 3-fold PC2 enhancement is particularly promising, as it matches the level shown in studies to nearly suppress cystogenesis while remaining within the safe, non-toxic range. Maintaining this balance of enhancing polycystin expression without exceeding physiological thresholds is critical for ADPKD therapy, given that *PKD1* overexpression itself can paradoxically drive cystogenesis³⁶. Our PPR-eIF4G platform achieves this

precision by enabling tunable, mutation heterogeneity-independent upregulation, while avoiding overexpression risks.

b. PPR-eIF4G target sensitivity

Our study demonstrates that PPR-eIF4G mediated translational enhancement exhibits remarkable positional sensitivity, where even minor (~3nt) shifts in target sites can completely or significantly influence outcomes. This can be observed in PC2-PPR2 and PC2-PPR5 where large shifts in PC2 expression was found (3.0-fold vs. 1.7-fold) despite only a 3nt distance from PPR targeting sites. The strict spacial requirement suggests that PPR-eIF4G mediated translational enhancement operates on a non-canonical mechanism district from cap-dependent initiation, which relies on eIF4E binding to the 5'cap. This aligns with previous research demonstrating that PPR-eIF4G works independently of eIF4E, and instead primarily utilizes its eIF3-binding domain to recruit ribosomes²⁶. This novel mechanism for translation could provide explanations for the importance of PPR-eIF4G target specificity.

The positional constraints of PPR-eIF4G mediated translational enhancement offer many different mechanistic speculations. Translational enhancement may involve certain steric requirements for PPR-eIF4G to physically bridge the PPR-RNA complex with translational machinery. Shifting targeting site by 3nt could disrupt PPR-eIF4G or other translational initiation proteins' ability to "reach" critical factors or mRNA modifications (e.g. 5-methylcytosine m⁵C, N1-Methyladenosine m¹A)³⁷. Another possible explanation is that optimal PPR-eIF4G target positions avoid secondary structures or position of internal ribosome entry sites (IRES) in *PKD1/PKD2* mRNA, however a previous study found no correlations between these sites and optimal target positions²⁶.

The precise mechanism underlying PPR target position-dependent translational enhancement remains unclear and warrants further investigation. Elucidating this mechanism could greatly improve target site screening strategies and deepen our understanding of PPR-RNA interactions in translational regulation. Future studies should investigate the influence of mRNA modifications or other epitranscriptomic marks on PPR-eIF4G or directly examine PPR-eIF4G interactions with other translational initiation factors. By addressing these questions, we can uncover fundamental principles of PPR-eIF4G mediated translational control and refine their utility in mRNA-based therapeutics.

c. Discrepancy between mRNA and protein expression in PC1 from miR-200 blocking constructs

In this study, we observed a 4-fold increase in *PKD1* mRNA levels upon miR-200 inhibition upon transfection of PC1-PPR22, however found no parallel increase in PC1 protein expression. This unexpected dissociation between transcript abundance and protein output contrasts with prior mechanisms whereby miR-200 directly binds to the *PKD1* 3'UTR to suppress its translation and transcript expression^{10,38}. Additionally, studies have demonstrated that miR-200 overexpression decrease PC1 levels, and its knockdown elevates PC1 expression^{39,40}. Our findings suggest a more

complex paradigm where miR-200 may regulate PC1 through additional mechanisms beyond canonical miRNA gene suppression.

The robust upregulation of PKD1 mRNA without proportional increases in protein indicates that while PPR-eIF4G successfully enhanced RNA stability (potentially due to miRNA blockade), it failed to fully counteract miR-200's translational regulation. This phenomenon remains intriguing as no prior studies have examined the influence of miR-200 binding site blockade on PKD1 mRNA stability and protein output. We hypothesize that miR-200 may regulate PC1 through modulation of downstream translational machinery or stress responsive pathways. Notably, miR-200 also inhibits mTORC1 signaling by targeting key regulators (RS1/AKT, Rheb, HIF-1a), leading to global suppression of elF4G-mediated cap dependent translation⁴¹. This could be particularly significant in our experimental context, as the PPR-eIF4G system's translational enhancement mechanism depends precisely on eIF4G-mediated ribosomal recruitment. We therefore propose that miR-200, though displaced from PKD1 binding, may directly interact with eIF4G modulators and counteract its function. Another non-exclusive possibility is that miR-200 may influence membrane polarity, thus similarly affecting membrane protein (including PC1) stability and translation. miR-200 maintains epithelial integrity by repressing EMT transcription factors (ZEB1/2) and preserving cell polarity⁴². Since PC1 is a transmembrane protein, loss of epithelial polarity due to miR-200 dysregulation could indirectly downregulate PC1 via cellular stress responses.

Taken together, the discrepancy between *PKD1* mRNA transcript and protein levels suggests miR-200 regulates PC1 through both direct and indirect mechanisms. Future studies should assess downstream miR-200 targets to elucidate observed translational suppression. Our findings highlight the complexity of miRNA blocking strategies in *PKD1* regulation.

IV. Conclusion

This study demonstrates the therapeutic potential of designer PPR-mediated translational enhancement in upregulating *PKD1* and *PKD2*, key genes implicated in ADPKD. Our findings reveal critical mechanistic insights into PPR-eIF4G's positional sensitivity, suggesting stringent spacial requirements, where even minor (3nt) shifts in target sites dramatically influence enhancement efficiency. The unexpected discrepancy between mRNA and protein levels in miR-200 blocking constructs led us to propose a speculative model where miR-200 may influence *PKD1* expression both though direct mRNA targeting, and indirect modulation of upstream regulators or co-factors. These findings establish PPR-eIF4G as a versatile tool for gene upregulation while underscoring the complexity of translational control mechanisms.

This study highlights several critical avenues for future investigation. Firstly, given PPR-eIF4G's positional sensitivity, systematically mapping optimal target positions between PKD1 and PKD2 mRNA could result in more potent translational upregulation. In conjunction, structural and functional interaction studies of PPR-eIF4G can reveal mechanistic insights to establish guidelines for optimal target section. Secondly, for uORF-blocking constructs in this study, we could not determine whether observed effects resulted from blocking by PPR alone, or genuine eIF4Gmediated translational enhancement. This distinction should be addressed in future work though testing of eIF4G-less PPR variants to determine whether blocking and effector-mediated translational enhancement synergies are possible. Thirdly, systematic evaluation of alternative translational activators including optimized eIF4G truncations, or other translational activators (e.g. YTHDF1, METTLE3) may identify more potent or positionally flexible effectors for PKD1/PKD2 upregulation. Finally, therapeutic applications and validation in ADPKD-relevant models remains critical. A rigorous evaluation of PPR-eIF4G's capacity to restore PKD1/PKD2 protein expression and rescue cellular phenotypes in ADPKD animal models is essential to establish its therapeutic potential. By systematically addressing these questions, we can develop PPR proteins into a more robust, modular platform for precise gene modulation.

This work advances our understanding of PPR-mediated translational control while providing a foundation for developing RNA-targeted therapies. Through continued mechanistic exploration and therapeutic optimization, PPR technology may emerge as a novel and powerful therapy for ADPKD and other disorders of haploinsufficiency.

V. Materials and Methods

a. Construction of programmable PPR protein gene

The PPR protein expression vector was designed to recognize a 12-nuclotide sequence on PKD/PKD2 RNA. Designer PPR proteins were constructed using a two-step Golden Gate assembly with the PPR3.0 scaffold, as previously described by Yagi et al²¹. A total of 144 intermediate plasmids encoding two PPR proteins were chemically synthesized. Each intermediate plasmid contained PPR motifs that recognized a dinucleotide pair. The PPR gene was assembled using intermediate plasmids, and a modified pFUS B1 vector (#31018, Addgene) with using Bpil and T4-DNA ligase via golden gate reaction. Reaction mixture contained 20ng of respective Tw plasmid, 1 µL 10×ligase buffer (New England Biolabs, Ipswich, MA, USA), 0.5 µL Bpil (Thermo Fisher Scientific, Waltham, MA, USA), 0.5 µL Quick ligase (New England Biolabs), and 25 ng of pFUS_B1 plasmid. The reaction mixture was placed in a thermal cycler with the following cycling conditions: 15 cycles of 37°C (5 min, digestion) and 16°C (7 min, ligation). Then, 0.4 µL Bpil was added to reaction mixture and incubated at 37°C for 30 min then 75°C for 6 min to digest residual plasmids. The mixture was further incubated at 37°C for 15 min with 0.4 µL of 1 mM ATP and plasmid-safe nuclease (Epicentre-Lucigen, Middleton, WI, USA) to degrade remaining linear fragments. Post assembly, 1 µL of reaction mixture was transformed into XL1-Blue competent cells and cultured on LB agar containing 50 µg/mL spectinomycin. Plasmids were extracted using Gen Elute HP Plasmid Miniprep Kit (Sigma-Aldrich, St. Louis, MO, USA). To screen insertion of PPR gene into pFUS_B1 vector, colony PCR was performed using GoTaq Master Mix (Promega, Madison, WI, USA), and size of insert was verified via agarose gel electrophoresis. The size and sequence of the insert and expression vector was further verified via restriction enzyme Xbal and Ndel cleavage and Sanger sequencing.

b. Construction of PPR-eIF4G fusion expression vector

Following construction of designer PPR vector, two intermediate plasmids containing $3\times FLAG$ tag, and another with eIF4G fragment was cloned into modified pFUS_B1 vectors. The truncated eIF4G fragment (607–1600 aa) used was based on a previously established construct^{26,27}. The PPR-eIF4G expression vector was assembled using $3\times FLAG$ tag, PPR, and eIF4G fragment pFUS_B1 plasmids and a modified pRL-CMV (#E2261; Addgene) with using *Esp3I* and T4-DNA ligase via golden gate reaction. Reaction mixture contained 20ng of each $3\times FLAG$ tag, PPR, and eIF4G fragment pFUS_B1 plasmids,0.2 μ L $10\times ligase$ buffer (New England Biolabs), 0.1μ L *Esp3I* (Thermo Fisher Scientific), 0.1μ L Quick ligase (New England Biolabs), and 15 ng of pRL-CMV plasmid. The reaction mixture was placed in a thermal cycler with the following cycling conditions: 15 cycles of 37°C (5 min, digestion) and 16°C (7 min, ligation). Then, 0.1μ L Esp3I, 0.25μ L 10 mM DTT, and 0.25μ L $10\times Tango$ buffer was added to reaction mixture and incubated at 37°C for 60 min then 80°C for 5 min. Post assembly, 1μ L of reaction mixture was transformed into XL1-Blue competent cells and cultured on LB agar containing 50μ g/mL ampicillin. Plasmids were extracted using Gen Elute HP Plasmid Miniprep Kit (Sigma-Aldrich). The sequence of the insert and expression vector was verified Sanger sequencing.

c. Cell culture and cell transfection

HEK293T cells were cultured in Dulbecco's modified Eagle's medium (DMEM; FUJIFILM Wako, Osaka, Japan), 10% fetal bovine serum (FBS; Gibco, Thermo Fisher Scientific), and penicillin–streptomycin (Gibco, Thermo Fisher Scientific) at 37 °C with 5% CO₂. HEK293T cells (ATTC CRL-3216; ATTC, Manassas, VA, USA) were seeded at 1.5x10⁵ cells per well in 12-well plates one day before transfection. HEK293T cells were transfected at 70-80% confluence using 100ng of respective PPR-eIF4G, and Lipofectamine 3000 Transfection Reagent (Thermo Fisher Scientific). Cells were then incubated for 48hrs at 37 °C with 5% CO2 before harvesting.

d. RNA extraction and cDNA synthesis

For total RNA collection, cells were homogenized in TRIzol Reagent (Thermo Fisher Scientific) followed by RNA purification using Direct-zol RNA Microprep Kit (Zymo Research, Irvine, CA, USA) according to the manufacturer's protocol. RNA purity and quality was assessed by spectrophotometry (A260/A280 ratio >1.8). cDNA was synthesized in 20µl reaction mixture containing 3µg of total RNA, 6µL nuclease-free water, and 4µL Maxima cDNA H Minus Synthesis Master Mix (5×; Thermo Fisher Scientific). The reaction mixture was incubated at 25°C for 10 min, 50°C for 25 min, then 85°C for 5 min. cDNA was stored at –80 °C or immediately used in RT-qPCR reaction.

e. Real-time quantitative polymerase chain reaction (RT-qPCR)

RT-qPCR was used to assess relative expression of PKD1 and PKD2 RNA. RT-qPCR was performed in quadruplicates using sample cDNA as a template with SYBR Green qPCR Kit. Each 20ul reaction mixture contained 500nM of forward and reverse primer, 10ng of cDNA, and 10µl of SYBR Green Universal Master Mix (2x; Applied Biosystems, Thermo Fisher Scientific). Cycling conditions were 95°C for 2 min, followed by 40 cycles of 95°C (15 sec, melting) and 60°C (1 min, annealing). Amplification curves of PKD1, PKD2, and β-actin were generated to calculate relative RNA expression via $\Delta\Delta$ Ct method. Normalized threshold cycle number (Δ Ct) was obtained by subtracting cycle threshold (Ct) values of sample and housekeeping gene (β-actin). ΔΔCt was derived by comparing Δ Ct values to untransfected control cells, while fold-change expression was calculated as $2^{-\Delta Ct}$. Primer efficiency was validated by melt and standard curve analysis. The following Primers were used: PKD1_Fw (5'-tctcaggcctccacgctg-3'), PKD1_Rv (5'-acaatggacgggtcactgag-3'), PKD2 Fw (5'-tccaagattgacgccgtgat-3'), PKD2 Rv (5'-gtcacgacccagcctttcat-3'), β-actin Fw (5'ccctggagaagagctacgag -3'), β-actin Rv (5'- aggtagtttcgtggatgcca -3'). Primers were designed using NCBI BLAST-Primer tool. Design parameters set to maintain amplicon sizes of 120±30 bp for high replication efficiency, and to flank an intronic sequence for differentiation between endogenous transcripts and potential genomic DNA contamination.

f. Western blot analysis

Cells were lysed in RIPA lysis buffer (20 mM HEPES pH 7.5, 1% IGEPAL CA-630, 0.1% SDS, 0.5% Deoxycholic acid, 150 mM Sodium Chloride) supplemented with protease and phosphatase inhibitor cocktail (WSE-7420 EzRIPA Lysis Kit, ATTO, Tokyo, Japan). Lysates were centrifuged at 16,000× g for 10 min at 4°C to remove cellular debris. Total protein concentration was measured using a

bicinchoninic acid assay (BCA) kit (Thermo Fisher Scientific). Equal protein amounts were resolved using SDS-PAGE using 7.5% polyacrylamide gel (ATTO) and transferred onto PVDF membranes using either (1) semi-dry system in EzFast Blotting Buffer (Atto Corporation) at 18 V for 30 min, or (2) wet transfer system in Tris-glycine buffer (25 mM Tris, 192 mM glycine, 10% methanol, pH 8.3) at 20 V for 3hrs. The following primary and secondary antibodies were used: Anti-PKD1 polyclonal antibody (PA5-115779, Thermo Fisher Scientific; 1:1000), Anti-PK2 polyclonal antibody (PA5-118167, Thermo Fisher Scientific; 1:500), Anti-FLAG M2 monoclonal antibody (F3165, Sigma-Aldrich; 1:1000), Beta Actin antibody (#CL594-60,008, proteintech, Tokyo, Japan) Goat Anti-Mouse IgG (#ab6789, Abcam; 1:2000), and Goat Anti-Rabbit IgG (#ab6721, Abcam; 1:10,000). All antibodies were diluted in 5% non-fat dry milk and incubated with membranes at 4°C overnight (primary) or room temperature for 1 hr (secondary). Chemiluminescence was visualized with Western Lightning Plus-ECL reagent (Revvity, Waltham, MA, USA) and imaged using ChemiDoc™ Touch instrument (Bio-Rad). For antibody removal, PDVF membranes were stripped with mild stripping buffer (0.2 M glycine, 0.1% SDS, 1% Tween-20, pH 2.2). Membranes were washed with TBST and re-blocked with 5% non-fat dry milk before subsequent re-probing with control protein antibody (β-actin). Protein band intensities were visualized using Bio-Rad ChemiDoc Imaging System (Bio-Rad) and were analyzed with Image Lab Software (v6.1, Bio-Rad). Target protein band intensity was compared to β -actin as the loading control.

g. Enzyme linked immunoassay (ELISA) for polycystin-1 and polycystin-2

HEK293T cells were harvested 48hrs after transfection of PPR-eIF4G. Human polycystin-1 and polycystin-2 ELISA kits (mlBio, Shanghai, China) were used. Cells were lysed in RIPA lysis buffer supplemented with protease and phosphatase inhibitor cocktail. Measured using BCA, protein concentration was adjusted to 0.4 µg/ml for each ELISA reaction. The ELISA was performed according to manufacturer's protocol. Addition of stop solution induced a colorimetric change quantified with spectrophotometric measurement at 450 nm. Polycystin-1 concentration was interpolated from the standard curve constructed with Polycystin-1 ELISA kit standards.

h. Statistical analysis

All constructs were compared to mock (empty vector)-transfected controls with a 2-tailed student's t-test. Significance threshold was set at p < 0.05.

VI. Bibliography

- 1. Chapman, A. B. *et al.* Autosomal-dominant polycystic kidney disease (ADPKD): executive summary from a Kidney Disease: Improving Global Outcomes (KDIGO) Controversies Conference. *Kidney Int* **88**, 17–27 (2015).
- 2. Barua, M. et al. Family History of Renal Disease Severity Predicts the Mutated Gene in ADPKD. Journal of the American Society of Nephrology **20**, 1833–1838 (2009).
- 3. Boucher, C. & Stanford, R. Autosomal dominant polycystic kidney disease (ADPKD, MIM 173900, *PKD1* and *PKD2* genes, protein products known as polycystin-1 and polycystin-2). *European Journal of Human Genetics* vol. 12 347–354 Preprint at https://doi.org/10.1038/sj.ejhg.5201162 (2004).
- 4. Al-Bhalal, L. & Akhtar, M. *Molecular Basis of Autosomal Dominant Polycystic Kidney Disease*.
- 5. Lanktree, M. B., Haghighi, A., Di Bari, I., Song, X. & Pei, Y. Insights into autosomal dominant polycystic kidney disease from genetic studies. *Clinical Journal of the American Society of Nephrology* **16**, 790–799 (2021).
- 6. Rossetti, S. *et al.* Incompletely penetrant *PKD1* alleles suggest a role for gene dosage in cyst initiation in polycystic kidney disease. *Kidney Int* **75**, 848–855 (2009).
- 7. Bushati, N. & Cohen, S. M. MicroRNA functions. *Annual Review of Cell and Developmental Biology* vol. 23 175–205 Preprint at https://doi.org/10.1146/annurev.cellbio.23.090506.123406 (2007).
- 8. Hajarnis, S. *et al.* MicroRNA-17 family promotes polycystic kidney disease progression through modulation of mitochondrial metabolism. *Nat Commun* **8**, (2017).
- 9. Sun, H. *et al.* MicroRNA-17 post-transcriptionally regulates polycystic kidney disease-2 gene and promotes cell proliferation. *Mol Biol Rep* **37**, 2951–2958 (2010).
- 10. Patel, V. et al. MicroRNAs regulate renal tubule maturation through modulation of *PKD1*. Journal of the American Society of Nephrology **23**, 1941–1948 (2012).
- 11. Yheskel, M., Lakhia, R., Cobo-Stark, P., Flaten, A. & Patel, V. Anti-microRNA screen uncovers miR-17 family within miR-17~92 cluster as the primary driver of kidney cyst growth. *Sci Rep* **9**, (2019).
- 12. Wang, J., Liu, J. & Guo, Z. Natural uORF variation in plants. *Trends in Plant Science* vol. 29 290–302 Preprint at https://doi.org/10.1016/j.tplants.2023.07.005 (2024).

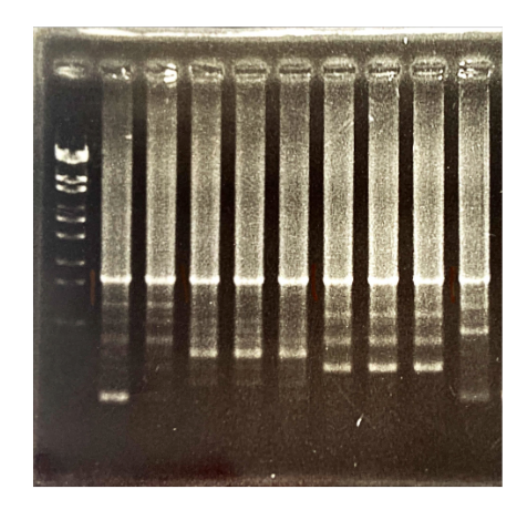
- 13. Chen, L., Gao, X., Liu, X., Zhu, Y. & Wang, D. Translational regulation of *PKD1* by evolutionarily conserved upstream open reading frames. *RNA Biology* vol. 22 1–12 Preprint at https://doi.org/10.1080/15476286.2024.2448387 (2025).
- 14. Yang, J. *et al.* Translational up-regulation of polycystic kidney disease protein *PKD2* by endoplasmic reticulum stress. *FASEB Journal* **27**, 4998–5009 (2013).
- 15. Davies, B. The technical risks of human gene editing. *Human Reproduction* vol. 34 2104–2111 Preprint at https://doi.org/10.1093/humrep/dez162 (2019).
- 16. Lee, E. C. *et al.* Discovery and preclinical evaluation of anti-miR-17 oligonucleotide RGLS4326 for the treatment of polycystic kidney disease. *Nat Commun* **10**, (2019).
- 17. Hedaya, O. M. *et al.* Secondary structures that regulate mRNA translation provide insights for ASO-mediated modulation of cardiac hypertrophy. *Nat Commun* **14**, (2023).
- 18. Agrawal, N. et al. RNA Interference: Biology, Mechanism, and Applications. *Microbiology and Molecular Biology Reviews* **67**, 657–685 (2003).
- 19. Manna, S. An overview of pentatricopeptide repeat proteins and their applications. *Biochimie* vol. 113 93–99 Preprint at https://doi.org/10.1016/j.biochi.2015.04.004 (2015).
- 20. Barkan, A. *et al.* A Combinatorial Amino Acid Code for RNA Recognition by Pentatricopeptide Repeat Proteins. *PLoS Genet* **8**, (2012).
- 21. Yagi, Y., Hayashi, S., Kobayashi, K., Hirayama, T. & Nakamura, T. Elucidation of the RNA Recognition Code for Pentatricopeptide Repeat Proteins Involved in Organelle RNA Editing in Plants. *PLoS One* **8**, (2013).
- 22. Bernath-Levin, K. *et al.* Cofactor-independent RNA editing by a synthetic S-type PPR protein. *Synth Biol* **7**, 1–11 (2021).
- 23. Barkan, A. *et al.* A Combinatorial Amino Acid Code for RNA Recognition by Pentatricopeptide Repeat Proteins. *PLoS Genet* **8**, (2012).
- 24. McDowell, R., Small, I. & Bond, C. S. Synthetic PPR proteins as tools for sequence-specific targeting of RNA. *Methods* **208**, 19–26 (2022).
- 25. Yagi, Y. et al. Construction of a Versatile, Programmable RNA-Binding Protein Using Designer PPR Proteins and Its Application for Splicing Control in Mammalian Cells. Cells 11, (2022).

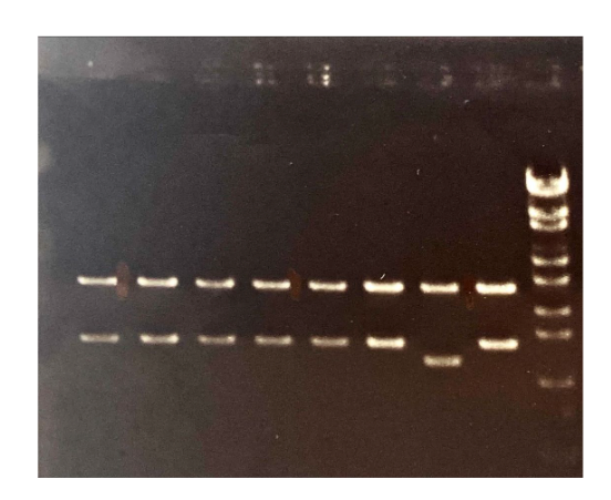
- 26. Ping, N., Hara-Kuge, S., Yagi, Y., Kazama, T. & Nakamura, T. Translational enhancement of target endogenous mRNA in mammalian cells using programmable RNA-binding pentatricopeptide repeat proteins. *Sci Rep* **14**, (2024).
- 27. Kobayashi, T., Yagi, Y. & Nakamura, T. Development of Genome Engineering Tools from Plant-Specific PPR Proteins Using Animal Cultured Cells. in 147–155 (2016). doi:10.1007/978-1-4939-4931-1 11.
- 28. Kozomara, A., Birgaoanu, M. & Griffiths-Jones, S. miRBase: from microRNA sequences to function. *Nucleic Acids Res* **47**, D155–D162 (2019).
- 29. McGeary, S. E. *et al.* The biochemical basis of microRNA targeting efficacy. *Science* (1979) **366**, (2019).
- 30. Hopp, K. *et al.* Functional polycystin-1 dosage governs autosomal dominant polycystic kidney disease severity. *Journal of Clinical Investigation* **122**, 4257–4273 (2012).
- 31. Li, A. *et al.* Human Polycystin-2 Transgene Dose-Dependently Rescues ADPKD Phenotypes in *PKD2* Mutant Mice. *American Journal of Pathology* **185**, 2843–2860 (2015).
- 32. Gainullin, V. G., Hopp, K., Ward, C. J., Hommerding, C. J. & Harris, P. C. Polycystin-1 maturation requires polycystin-2 in a dose-dependent manner. *Journal of Clinical Investigation* **125**, 607–620 (2015).
- 33. Rogers, K. A. *et al.* Differences in the timing and magnitude of *PKD1* gene deletion determine the severity of polycystic kidney disease in an orthologous mouse model of ADPKD. *Physiol Rep* **4**, (2016).
- 34. Rossetti, S. *et al.* Incompletely penetrant *PKD1* alleles suggest a role for gene dosage in cyst initiation in polycystic kidney disease. *Kidney Int* **75**, 848–855 (2009).
- 35. Mullard, A. Gene therapy community grapples with toxicity issues, as pipeline matures. *Nature reviews. Drug discovery* vol. 20 804–805 Preprint at https://doi.org/10.1038/d41573-021-00164-x (2021).
- 36. Thivierge, C. *et al.* Overexpression of *PKD1* Causes Polycystic Kidney Disease. *Mol Cell Biol* **26**, 1538–1548 (2006).
- 37. Roy, B. Effects of mRNA Modifications on Translation: An Overview. in *Methods in Molecular Biology* vol. 2298 327–356 (Humana Press Inc., 2021).

- 38. Sachin Hajarnis. *Polycystic Kidney Disease*. *Polycystic Kidney Disease* (Exon Publications, 2015). doi:10.15586/codon.pkd.2015.
- 39. Wessely, O. & Tran, U. Small RNAs Have a Big Effect on Polycystic Kidney Disease. Journal of the American Society of Nephrology 23, 1909–1910 (2012).
- 40. Bi, K. et al. Original Article Effect of MiR-200 on Autosomal Polycystic Nephropathy in Rats. Int J Clin Exp Pathol vol. 9 www.ijcep.com/ (2016).
- 41. Wu, S. Q. *et al.* MicroRNA-200c affects bladder cancer angiogenesis by regulating the Akt2/mTOR/HIF-1 axis. *Transl Cancer Res* **8**, 2713–2724 (2019).
- 42. Wellner, U. *et al.* The EMT-activator ZEB1 promotes tumorigenicity by repressing stemness-inhibiting microRNAs. *Nat Cell Biol* **11**, 1487–1495 (2009).
- 43. Davis, M. W. & Jorgensen, E. M. ApE, A Plasmid Editor: A Freely Available DNA Manipulation and Visualization Program. *Frontiers in Bioinformatics* **2**, (2022).

VII. Supplementary information

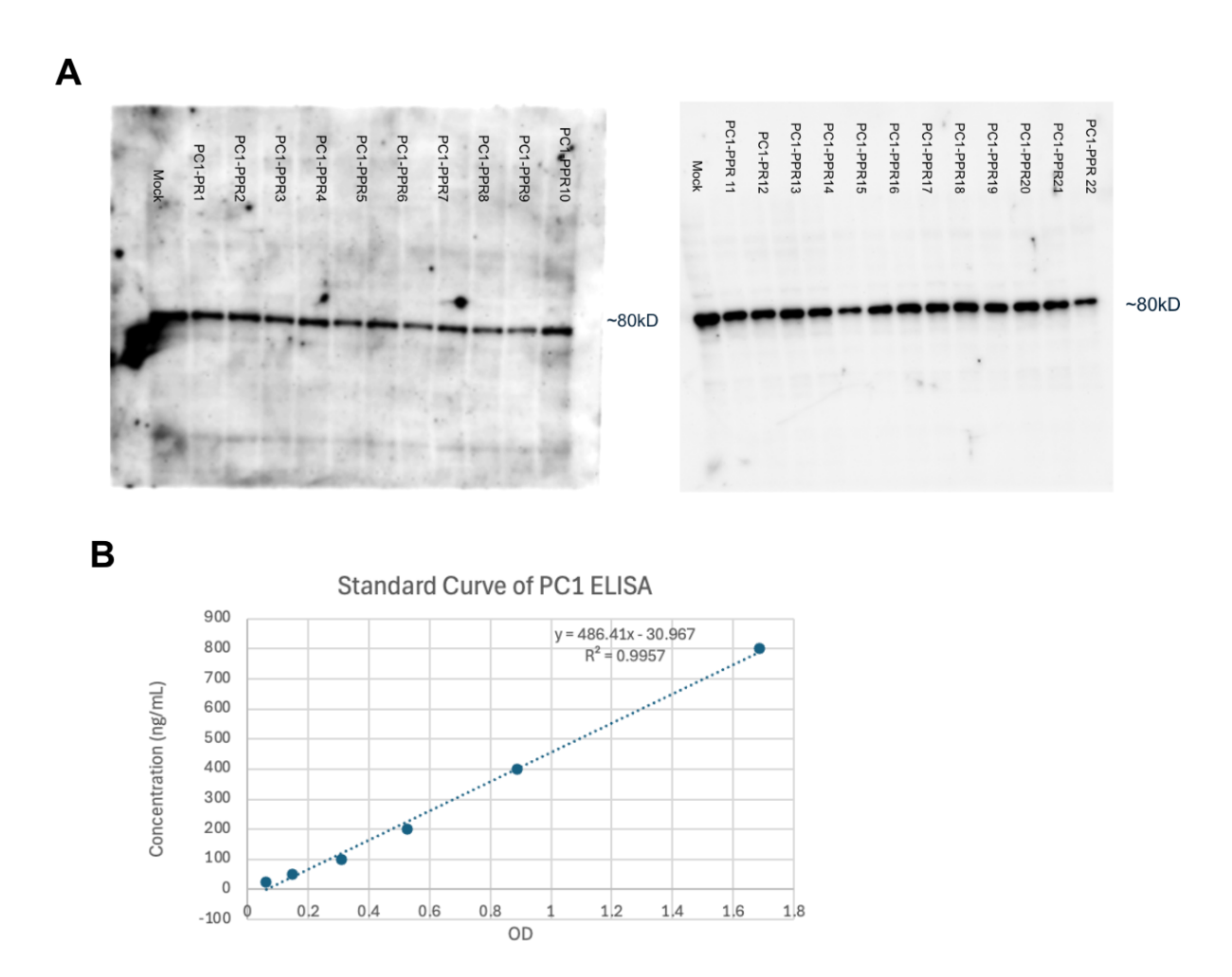
A B



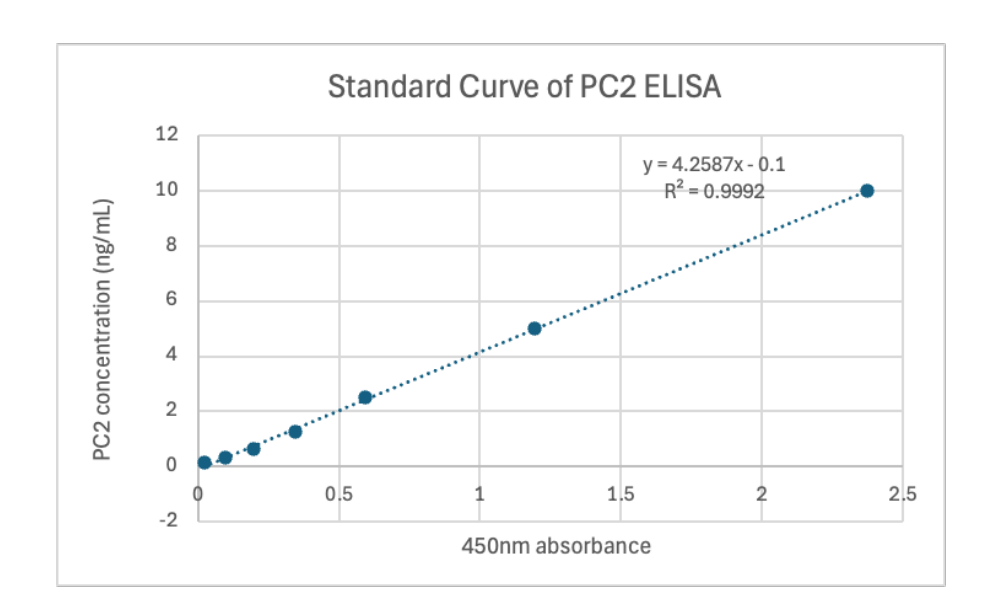


Supplementary Figure 1. Confirmation of PPR-eIF4G expression vectors

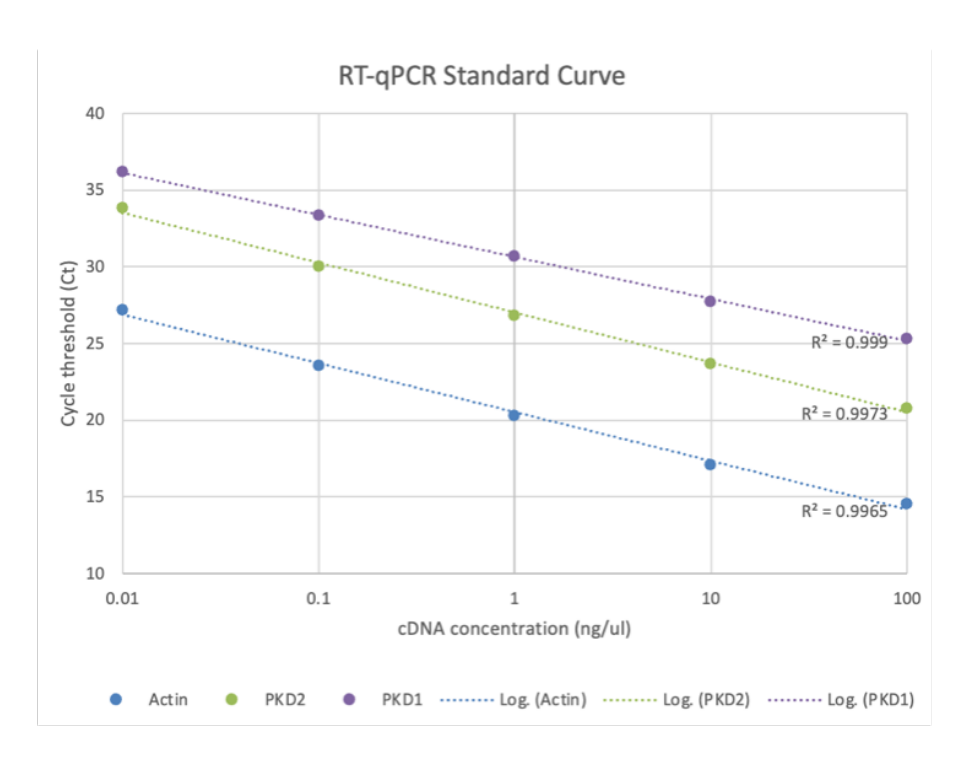
(A) Gel electrophoresis analysis of PPR insert following plasmid/colony PCR using PCR8 primers. Insert size confirmation was conducted following the first round of golden gate assembly. **(B)** Gel electrophoresis analysis following Xbal and Ndel restriction enzyme digestion of PPR vector. Size of digestion product was calculated using ApE Plasmid Editor software⁴³.



Supplementary Figure 1. Western blot of PC1 and ELISA standard curve **(A)** Western blot analysis of *PKD1* using anti-polycystin-1 antibody. Unexpected 80kD band was detected with no band at predicted molecular weight of full-length PC1 (~440kD) **(B)** ELISA standard curve for PC1 used to interpolate sample PC1 concentration.



Supplementary Figure 3. ELISA standard curve for PC2 used to interpolate sample PC2 concentration.



Supplementary Figure 4. Primer efficiency verification; qPCR standard curve *for PKD1*, *PKD2*, and β -actin primers.